UNIVERSITY OF CALIFORNIA SAN DIEGO

A Targeted Approach to Increasing Glucose Uptake and Metabolism of Adipocytes

A thesis submitted in partial satisfaction of the requirements
for the degree Master of Science

in

Chemistry

by

Hancy A. Barnes

Committee in charge:

Professor Kamil Godula, Chair
Professor Philip Gordts, Co-Chair
Professor Galia Debelouchina

2024

The thesis of Hancy A. Barnes is approved, and it is acceptable in quality form for publication on microfilm and electronically.

UNIVERSITY OF CALIFORNIA SAN DIEGO

2024

DEDICATION

I dedicate this thesis to my mom, LeiLani Barnes Collins; whose courage and fight against diabetes inspired me to dive into unfamiliar territory and strive to make an impact towards a cure.

TABLE OF CONTENTS

LIST OF ABBREVIATIONS

3-Isobutyl-1-methylaxanthine (IBMX)

Bovine Calf Serum (BCS)

Delta like non-canonical Notch ligand 1 (DLK1)

Dulbecco's Modified Eagle's Medium (DMEM)

Dulbecco's Phosphate Buffered Saline (DPBS)

Extracellular Matrix (ECM)

Fetal Bovine Serum (FBS)

Free Fatty Acids (FFA)

Glycosaminoglycan (GAG)

Growth Factors (GF)

Heparan Sulfate (HS)

HS Binding Proteins (HSBP)

Heparan Sulfate Proteoglycans (HSPG)

Immunofluorescence (IF)

Mouse Embryonic Fibroblast (MEF)

N-deacetylase-N-sulfotransferase 1 (Ndst1)

Neo Proteoglycans (NeoPGs)

polyvinylidene difluoride (PVDF)

proliferator activated receptor gamma (Pparγ)

proteoglycans (PG)

Stromal Vascular Fraction (SVF)

Type II Diabetes (T2D)

White Adipose Tissue (WAT)

Wild Type (WT)

Wingless Type (Wnt)

LIST OF FIGURES

LIST OF FIGURES

LIST OF TABLES

LIST OF SUPPLEMENTAL FILES

Supplementary File 1: BarnesThesis_SupplementaryFigures.pdf

Figure 1: Permeabilized and non-permeabilized immunostaining of WT MEFs at day 0 and day of differentiation.

Figure 2: Flow cytometry gating strategy

Figure 3: Original photographs of differentiation with and without biotinylated anti-PDGFRα

Supplementary File 2: BarnesThesis_TyrPEGamineLinker

Supplementary File 3: BarnesThesis_mSA_Isolation-Purification

ACKNOWLEDGEMENTS

I'd like to acknowledge Professor Kamil Godula for his support and guidance throughout this entire process. I've learned a lot in the last 18 months, and I truly appreciate the time and patience taken for each revision of this document. I'd like to thank the efforts of all current and former lab members. Special thanks to Pravinkumar Choudhary, Julliana Follmar, and Alexander Parmele for developing Hep-mSA conjugates; Garland Jackson, Phoebe Murayama, Sarah Wax and Nathan Le for their helping hands and words of wisdom.

I'd like to acknowledge Asst Professor Philip L. S. M. Gordts and Professor Jeffrey D. Esko for being rock stars in the "glyco-community" and welcoming me into their lab as a collaborator. Thanks to all current lab members, I always felt included. Special thanks to Chelsea Painter, Stephanie Leal, Nathan Thomas, Chung-Jui (Raymond) Yu, Jessica Perez, Jessica Pihl, and Cameron Pormir for offering their expertise and words of encouragement to continue in the face of failure.

I'd like to acknowledge Dr. Francesca Boscolo from the Sanford Consortium of Degenerative Medicine and Dr. Lakshmi Nagarojan from Bio-Techne for taking time to help with my staining protocols. Without their help, my project would not have proceeded as quickly as it had.

I'd like to acknowledge UCSD School of Medicine Microscopy Core Grant P30 NS047101 for providing imaging equipment and training.

Results section II is coauthored with Pravinkumar Choudhary, Julianna Follmar and Alexander Parmele. The thesis author was the primary author of this section.

ABSTRACT OF THE THESIS

A Targeted approach to Increasing Glucose Uptake and Metabolism of Adipocytes

by

Hancy A. Barnes

Master of Science in Chemistry

University of California San Diego, 2024

Professor Kamil Godula, Chair
Professor Philip Gordts, Co-Chair

Diabetes is a chronic health condition that has reached global epidemic proportions and continues to increase with every passing year. There are two major types of diabetes: type 1 and type 2 diabetes (T2D); 90 percent of those living with this health condition have T2D. These individuals suffer from high blood glucose levels, which induces insulin resistance and eventual organ failure that leads to death. Current

therapeutic approaches to alleviate high glucose levels are limited to dieting, personally administered insulin injections, devices that release insulin, and blood glucose lowering pharmacological agents. We believe that glycocalyx remodeling could be a potential therapeutic to improve glucose homeostasis in individuals with T2D. We have generated evidence that heparan sulfate mimetics will alter the differentiation program of pre-adipocytes by modulating Wnt signaling. This results in adipocytes with increased glucose uptake and utilization independent of insulin secretion. In this current study, we aim to identify a targetable pre-adipocyte marker to selectively deliver our heparan sulfate mimetic. This marker will then be utilized to demonstrate that heparan sulfate mimetic addition during adipogenesis does not alter cell identity and function.

Introduction

Adipose tissue – its role in glucose metabolism and T2D

Adipocytes, the primary cells of adipose tissue, are specialized for the storage of fat. It is well established that adipocytes play a significant role in glucose metabolism and energy homeostasis[1]. The plasticity of adipocytes allows them to contract and expand with varying energy expenditure requirements; however, the capacity for these fat cells to expand is limited[2]. This limitation was realized as dietary requirements changed from farm-fresh to fried or fast foods with high-fat content and processed foods containing refined sugars (the western diet). The imbalance between caloric intake and energy expenditure causes excessive adiposity[3] and greatly contributes to the current obesity epidemic. Obesity is a leading cause of insulin resistance, which escalates the onset of Type II Diabetes[4] (T2D).

T2D is a long-term health condition that is characterized by the inability to regulate blood glucose (sugar) levels. A prominent diagnostic marker for T2D is insulin resistance, which is when cells no longer respond to insulin, a hormone secreted by the pancreas which helps regulate glucose levels in the blood (Figure 1). On a cellular level, insulin doesn't trigger a response from muscle, liver, or adipose tissue to utilize glucose from the blood[5]. Prolonged exposure to hyperinsulinemia conditions destroys pancreatic β-cells and dampens their capacity to secrete insulin. T2D has reached global epidemic proportions[6], and with the increasing prevalence of diabetes in young individuals[7], the decline of this health condition is not in sight. Currently, treatments for T2D include dieting, exercise, insulin injections, metformin, and newer pharmacological therapeutics - such as Ozempic and Mounjaro. Insulin injections provide an exogenous source of insulin to help

regulate blood glucose levels[8]. Metformin is an oral medication which suppresses liver gluconeogenesis[9],thereby reducing blood glucose levels. Ozempic and Mounjaro work two-fold, first by mimicking signaling hormones that release insulin and inhibit glucagon secretion, and secondly by slowing the rate of digestion which prompts the feeling of satiety[10]. The effects of these actions help to regulate overall blood glucose levels after a meal and help with weight loss. Although these current therapies are promising, they are not replacements for, and can be prescribed concomitantly with other T2D treatments like insulin or metformin. None of these therapies systemically treat the underlying cause of T2D – which is insulin resistance.

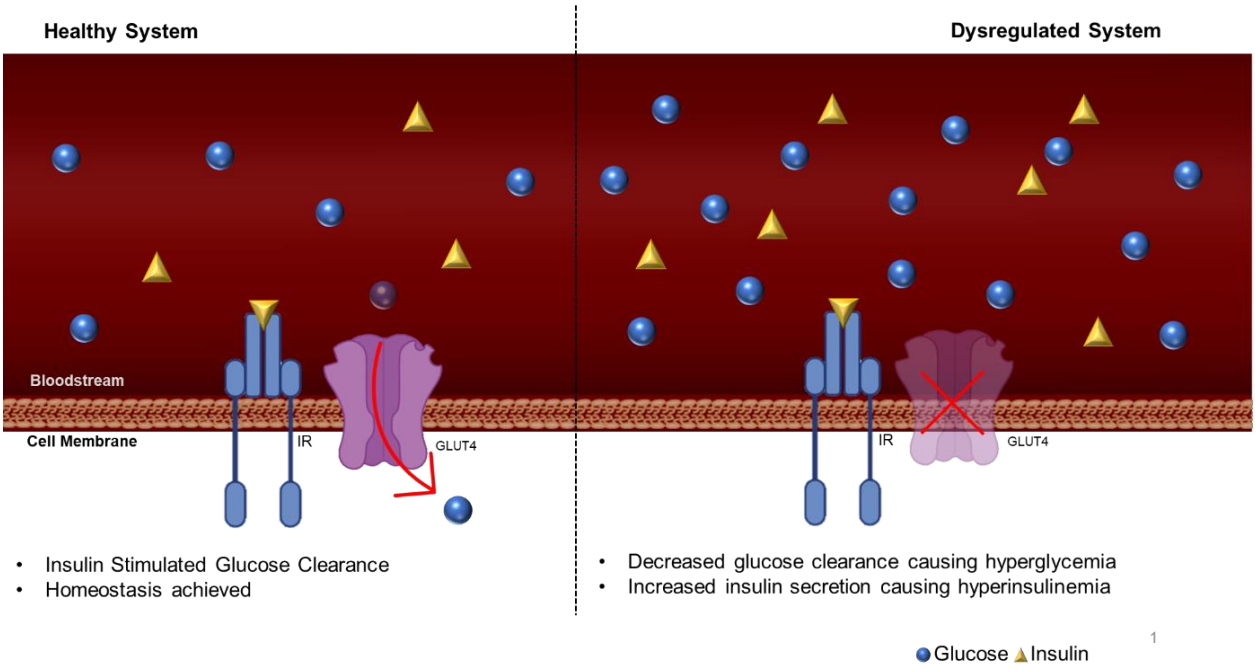

Figure 1: Depiction of Glucose Regulation in Healthy and T2D Systems
Heathy system: Insulin stimulates insulin receptors on the cell surface, glucose transporter 4 is translocated to the cell surface and facilitates the uptake of serum glucose into the cell. T2D System: Insulin stimulation does not trigger translocation of GLUT4 to the cell surface. Serum glucose and insulin levels rise, leading to β-cell death and insulin resistance.

Dysregulation of glucose homeostasis in obesity-induced metabolic disorders

Aside from T2D, adipose tissue dysregulation is implicated as the cause of many obesity-related metabolic disorders[11,12]. When caloric intake consistently exceeds energy expenditure, adipose tissue becomes hypertrophic. As adipose tissue expands, they become stress induced, inflamed, and insulin resistant, which is associated with the visceral deposition of adipocytes[11]. Abnormally high visceral fat storage is linked to an increased risk of heart disease, stroke and T2D[13].

The role of adipocytes in glucose metabolism and energy homeostasis

White adipose tissue (WAT) is considered a dynamic organ, and it is established that outside of storing lipids, adipose tissue is important for energy homeostasis, insulin signaling, and endocrine activity[14]. Adipose tissue is comprised of mature adipocytes and other cell types known as the stromal vascular fraction (SVF) that include precursors, preadipocytes, macrophages, dendritic, endothelial, T- and B- cells. Together, these cells construct the signaling cascades and interactions with the extracellular matrix (ECM) that defines the function of adipocytes[15].

Glucose metabolism and homeostasis are at the heart of the T2D condition. Glucose metabolism is the process in which our bodies break down carbohydrates into glucose (Figure 2), while glucose homeostasis refers to the delicate balance between glucose and insulin to maintain normal blood glucose levels. Adipocytes hold a critical function in both processes. After glucose is absorbed into the bloodstream, insulin is secreted from the pancreas into the bloodstream. Insulin binds to its receptor and this triggers Glucose Transporter 4 (GLUT4) to translocate to the cell surface to facilitate the movement of glucose into the cell[16]. Once in the cytosol of the adipocyte, glucose is

metabolized through glycolysis to generate ATP (energy) and triglycerides (potential energy). Adipocytes are most known for the storage triglycerides, which are housed in lipid droplets. The role adipocytes play in glucose homeostasis and the cell's endocrine functionality is appreciated in times of nutrient deficiency. During these times, lipolysis occurs in the lipid droplet by hydrolyzing triglycerides into glycerol and free fatty acids (FFA)[16]. These products are released into the bloodstream, and subsequently used as an energy source by other organs to perform other important processes. For instance, the liver uses glycerol as a precursor to generate glucose by the process of gluconeogenesis[16] and converts FFAs to ketone bodies which are used as an alternate energy source for the brain[17]. Notably, these are not the only two processes that are regulated by adipocytes, which demonstrates the complexities of this organ regarding overall health.

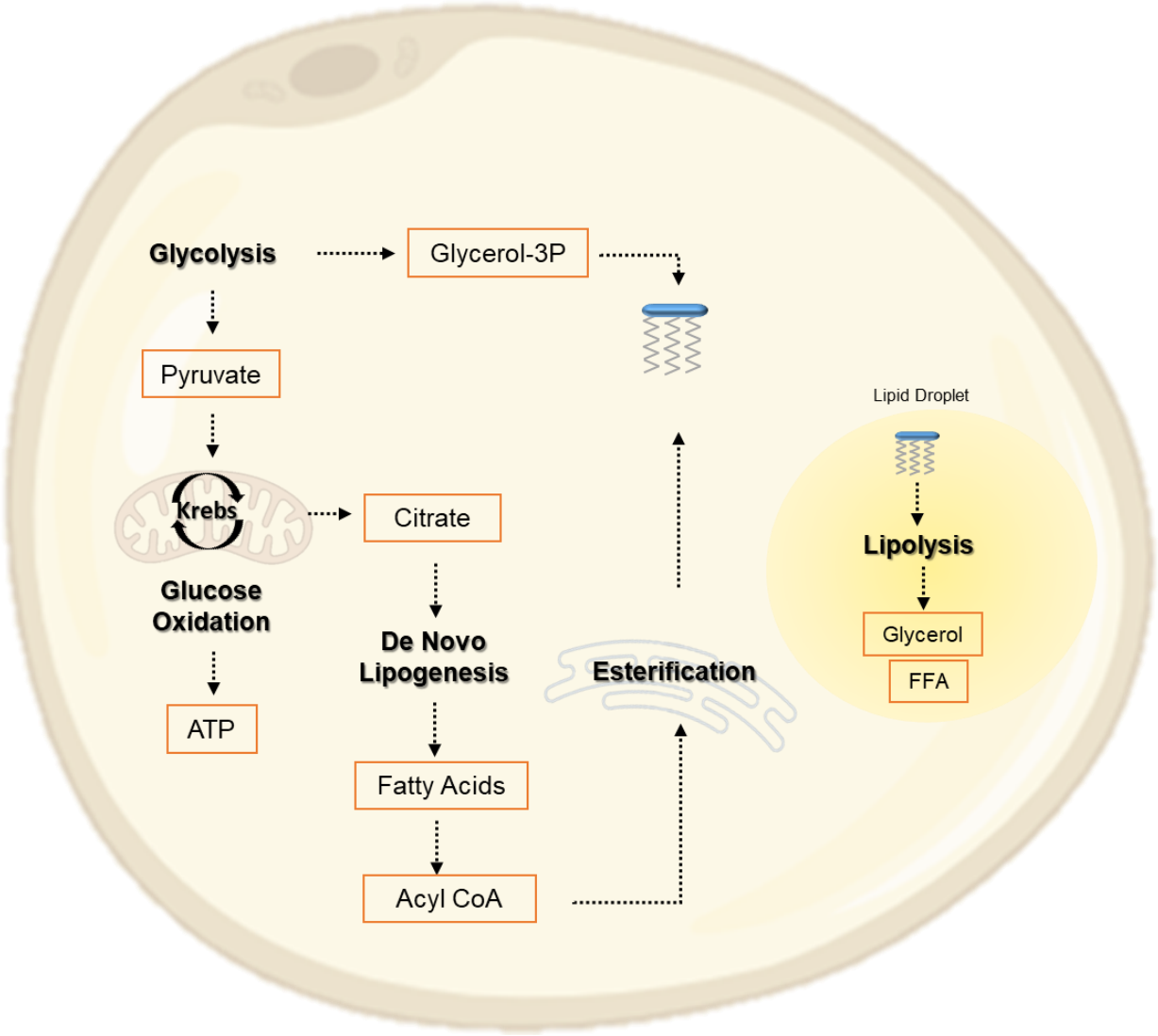

Figure 2: Glycolysis and Lipolysis processes in mature adipocytes.
Glycolysis is the breakdown of glucose into glycerol-3-phosphate (glycerol-3P), which constitutes the backbone of triglycerides and pyruvate, which goes through the Krebs cycle. The Krebs cycle will produce ATP and citrate. If insulin is present, it can stimulate de novo lipogenesis to produce fatty acids, which can be stored as triglycerides in lipid droplets. Lipolysis occurs in the lipid droplet where triglycerides are hydrolyzed and broken down into FFA and glycerol.

Since adipocytes have a high impact on glucose metabolism, targeting their precursors may provide a way to reprogram the attributes of mature adipocytes. Heparan Sulfate (HS) is a linear polysaccharide that is found abundantly as side chains attached to proteoglycans (PG) on the cell surface and comprises part of the glycocalyx. Due to

the varying sulfation domains and the net negative charge of HS, it has massive influences over many different signaling pathways which are still being uncovered. In this context, HS interacts with growth factors which affect cellular differentiation[18]. The preface to this work concludes that treating preadipocytes with a synthetic HS-mimetic in the early stage of cellular differentiation induces an altered metabolic set point of glucose uptake in mature adipocytes[19]. Cell surface glycocalyx remodeling is an underdeveloped pharmacological treatment approach; by conjugating HS to a preadipocyte specific antibody, glucose uptake in adipocytes could be enhanced independent of insulin. Overall, while current therapies target appetite and food intake, this method aims to increase cellular glucose uptake and could become a novel way to treat T2D.

Adipogenesis and the role of HS in regulating adipocyte metabolism

Adipogenesis is the process in which precursor mesenchymal stem cells (MCS) transition to fibroblastic preadipocytes that are committed to differentiate into mature adipocytes (Figure 3A)[14]. To study adipogenesis, the identification of committed adipocyte precursor cells is essential. It is well established that the expression of proliferator activated receptor gamma (Pparγ) is necessary for cellular differentiation to adipocytes and is widely used as the identifying marker of committed preadipocytes[14]. Just as adipogenic progenitor cells have identifying markers, so do pre- and mature adipocytes. It is important to note that these cells have different protein expressions depending on the stage of cellular differentiation. For instance, the expression of Delta-like non-canonical Notch ligand 1 (DLK1) is a biomarker for preadipocytes and is not found abundantly in mature adipocytes[14].

Currently, the most common system for studying adipogenesis is the NIH 3T3-L1 murine preadipocyte cell line, which rapidly differentiates into mature adipocytes upon hormone stimulation[20] (Figure 3B). These cells have the purest phenotype of adipocytes; however, after a number of passages the cells lose their differentiation efficiency[21]. Our lab previously used wild type (WT) and Ndst1-deficient ($Ndst1^{-/-}$) mouse embryonic fibroblasts (MEFs) to explore adipogenesis[19].

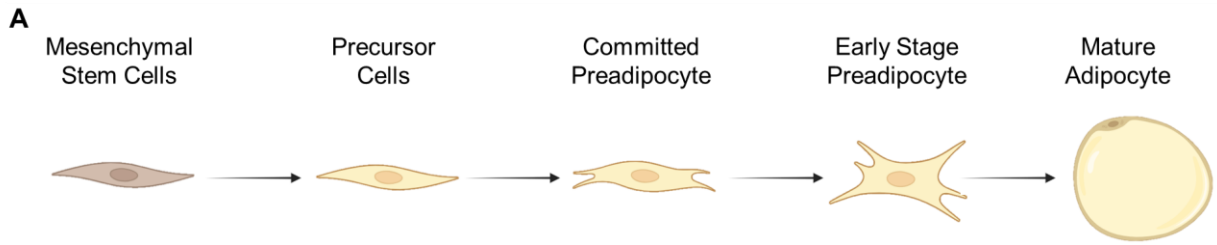

Figure 3: A. Adipogenesis – Natural Pathway from MSCs in the Body
Depiction of natural progression of MSC progressing into precursor cells, then into committed preadipocytes, where fibroblastic characteristics are observed. Committed preadipocytes continue to develop through cellular differentiation into mature adipocytes. **B. Modeling Adipogenesis In Vitro from NIH 3T3-L1/MEFs.** Positive adipogenic markers for different stages of adipogenesis. Timeline and conditional media for MEFs (black) and 3T3-L1 (red) are shown at the top and bottom of each column. 3T3-L1 cells have an additional media change to insulin media on Day 2 that is not shown here.

Figure 3 Continued

B

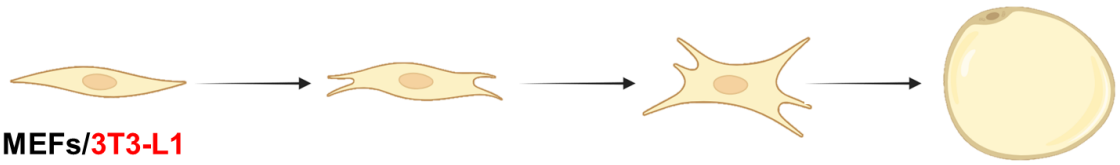

Positive Markers			
SEED/SEED	**Day 0/Day-1**	**Day 3/Day 0**	**Day 6+/Day 4+**
Sca-1, 3G5, HLA-ABC, ABCG2, NG2, CD10, CD13, CD29, CD34, CD44, CD49a, CD49b, CD49d, CD49e, CD55, CD59, CD71, CD73, CD90, CD105, CD120a, CD124, CD140a, CD140b, CD166	Sca-1, NG2, CD24, CD29, CD34, CD90, CS140a, CD140b, P2RX5, DLK1, GSTP1, LYRM1	Sca-1, NG2, CD24, CD29, CD34, CD90, CD140b, P2RX5, DLK1, GSTP1, LYRM1	CD10, CD13, CD34, CD36, CD55, CD59, CD65, CD120a
MEDIA: FBS/BCS	**Differentiation/BCS**	**Insulin/Differentiation**	**Insulin/Maintenance**

Cell surface glycans, such as HS, play an important role in regulation of signaling during development and in normal tissue function and have been implicated as factors in various diseases[22]. Prior work identified HS as regulators of signaling governing glucose homeostasis or inflammation during obesity and T2D[11].

HS is a negatively charged glycosaminoglycan (GAG) side chain linked to the serine or threonine residue of a protein core (Figure 4)[23]. The assembly of HS is initiated by xylosyltransferase, which attaches a xylose residue to the protein core. From there, a tetrasaccharide linker containing two galactoses (Gal), a glucuronic acid (GlcA) and a *N*-Acetylglucosamine (GlcNAc) is added to the xylose residue. The rest of the assembly is a tandem repeat of GlcA and GlcNAc, which is altered extensively by the addition of sulfation by sulfotransferases 1-4 and the epimerization of GlcA to iduronic acid (IdoA)[23].

Of the sulfotransferases, *N*-deacetylase-*N*-sulfotransferases (Ndst1-4) initiates the first N-sulfation modification on the GlcNac residue, followed by the 2-*O*-sulfation by heparan sulfate 2-*O*-sulfotransferases (HS2ST) on the IdoA or GlcA, then the 6-*O*-sufation of select GlcNac residues by heparan sulfate 6-O-sulfotransferases (HS6ST1-3), and finally the least abundant sulfation addition of 3-*O*-sulfation is added by heparan sulfate 3-*O*-sulfotransferases HS3ST1-6 on certain glucosamine (GlcN) and IdoA residues. Further modification of HS happens once it is secreted to the cell surface membrane[23]. The sulfation on HS isn't uniform throughout the chain but distributed in clusters of high and low sulfation domains[23], which gives HS its overall negative charge and is what ultimately attracts HS binding proteins[24]. It is important to note that the Ndst1 enzyme is a key contributor to HS sulfation, determining the overall extent of modification[25,26]. The heterogeneous nature of HS to bind to different proteins and interact with various motifs on and surrounding the cell surface[25], establishes its vast attributes and applications.

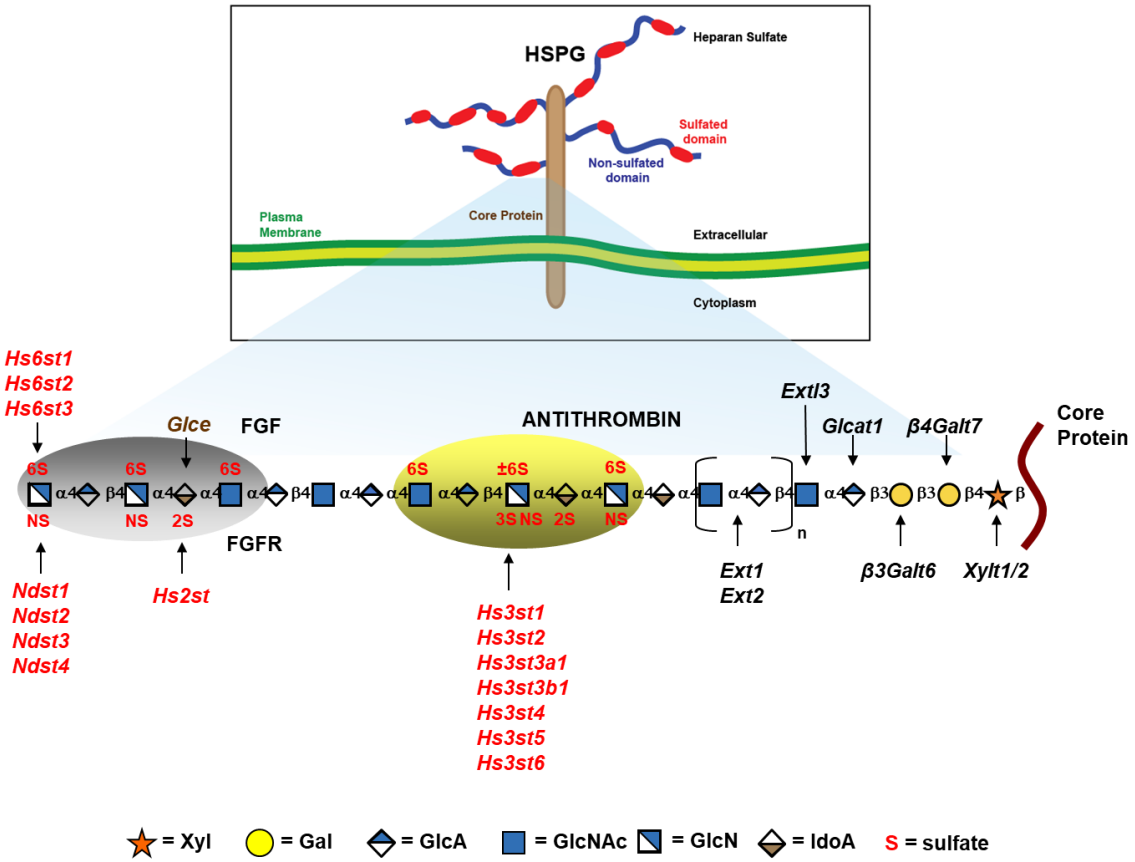

Figure 4: Heparan Sulfate Proteoglycan Structure
HS biosynthesis commences by the copolymerization of alternating N-acetylated glucosamine and glucuronic acid residues on a tetrasaccharide primer (glucuronic acid (GlcA)-galactose (Gal)-galactose-xylose (Xyl)-) that is covalently bound to a serine residue in the extracellular domain of the core proteins of membrane proteoglycans and extracellular matrix proteoglycans. The chains undergo various modifications as shown in the top of the figure by red shading. The modifications occur in clusters of variable length (sulfated domains), which are interspersed by unmodified domains (non-sulfated domains) indicated in blue. HS biosynthetic enzymes convert subsets of N-acetylated glucosamine (GlcNAc) residues to N-sulfoglucosamine units (catalyzed by members of the NDST family of enzymes), epimerization of nearby glucuronic acid residues to iduronic acid (IdoA) (catalyzed by a C5 epimerase [Glce]), and additional sulfation reactions at C6 of glucosamine units, C2 of uronic acids, and C3 of N-sulfoglucosamine units (catalyzed by HS6ST, HS2ST and HS3ST isozymes). The modified domains make up binding sites for protein ligands as depicted for antithrombin and FGF/FGFR.
Image adapted from Gordts and Esko[27]

To investigate the role of HS during adipogenesis our lab used MEFs that Gordts and co-workers isolated from genetically altered HS (Ndst1$^{-/-}$) mice. These MEFs produce adipocytes with low lipid storage and the same phenotype was observed in WT MEFs differentiated in the presence of soluble heparin[19], a highly sulfated version of HS. When

Heparin is added exogenously it can compete with HS for the binding of cell-surface signaling proteins[28]. Upon differentiation, FFA uptake, lactate production and other staples of adipogenesis were analyzed. What was found is that lipid uptake and the expression of GLUT4 between WT and HS deficient cells was not significantly different, and lactate – a byproduct of glycolysis – production was higher in WT cells. They concluded that the decrease in glucose uptake in HS-altered adipocytes was due to a switch in metabolism from glycolysis to fatty acid catabolism. Ultimately, through evaluating gene expression during differentiation, it was found that HS activity during early (Day 0-3) of adipogenesis was important in defining the metabolic set point of mature adipocytes (Figure 5)[19].

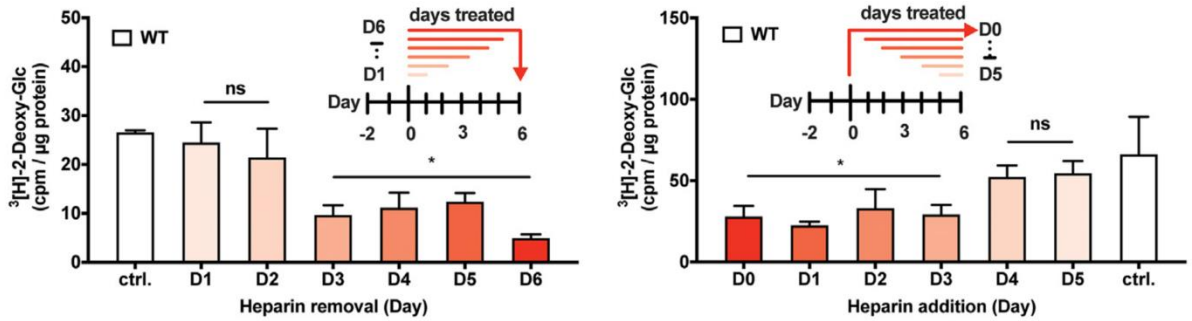

Figure 5: Heparan Sulfate Defines Metabolic Setpoint During Early Adipogenesis
All cells were treated with heparin starting at Day 0 of differentiation. Removal of heparin before day 3 did not evoke a change in glucose uptake (left) and the addition of heparin after Day 4 no longer modulates glucose uptake compared to the control. Image from Trieger et al[19].

The role of HS during adipogenesis was elucidated as the sequester of Wnts, which without interference from HS activates the frizzled/wnt signaling pathway that inhibits the destruction of β-catenin[19], a protein critical for embryonic cell proliferation and differentiation[29]. This signaling pathway is highly conserved and has been implicated as suppressing adipogenesis by inhibiting the adipogenic transcriptional factor cascade of CCAAT-enhancer-binding protein β (C/EBPβ), C/EBP-α and PPARγ[30], which is needed

for adipogenesis. Trieger et al. used HS inhibited cell models to show that genetic (Ndst1 deficient) and chemical (heparin treated) inhibition of HS produces a cell with decreased lipid accumulation (Figure 6). To investigate how HS was involved, glucose uptake and FFA uptake analysis was performed on WT and Ndst1$^{-/-}$ cells treated with exogenous heparin. Heparin is a GAG chain that is more highly sulfated with less variability than HS, for this reason, it is widely used in pharmaceuticals instead of HS[28]. In the context of Trieger's work, heparin was used to outcompete HS for interactions with growth factors (GF) and other HSBP. What was found is that glucose uptake of WT MEFs was significantly decreased to levels comparable to those of Ndst1$^{-/-}$ cells when treated with exogenous heparin, and upon insulin stimulation of these HS inhibited MEFs, there was no difference in the basal level of glucose when compared to untreated WT. This showed that the decrease in lipid accumulation was not due to impaired FFA uptake and HS acts independently of the insulin signaling pathway. It was hypothesized that the decrease in glucose uptake was attributed to the cell's metabolic switch from glycolysis to fatty acid-dependent oxidative metabolism (utilizing fats for energy). This hypothesis was validated through the analysis of lactate and palmitate production in the cells and the subsequent question of how HS prompts this switch was posed. From there, Trieger et al. treated cells with heparin during different days of differentiation to determine when HS activity was prominent. It was shown that the first three days of differentiation are crucial for heparin to reduce glucose uptake. Transcription factors were analyzed, and it was confirmed that genes closely related to Wnt superfamilies were upregulated in HS deficient cell models. Therefore, the conclusion was drawn that HS regulates adipogenesis by sequestering

Wnts away from the frizzled receptor and inhibiting the suppression of adipogenesis by β-catenin.

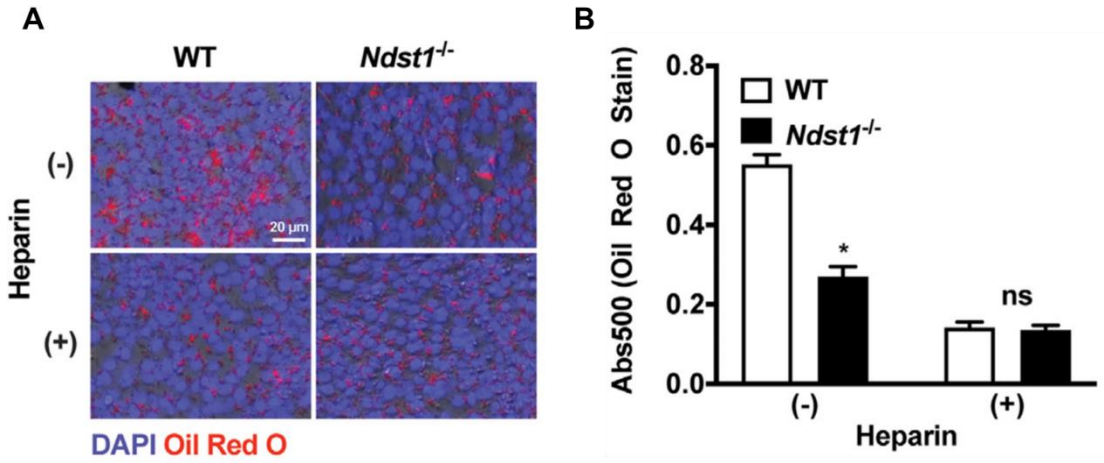

Figure 6: HS Deficiency Results in Low Accumulation of Lipids
A. Oil Red O stain of differentiated WT and Ndst1$^{-/-}$ adipocytes treated with or without heparin (100μg/mL). Nuclei visualized with DAPI. **B.** Quantified Oil Red O stain performed by elution of stain (two-way ANOVA, n = 3).

HS glycocalyx engineering to enhance glucose uptake in adipocytes

With the role of HS uncovered, Trieger et al. sought to attenuate Wnt signaling through the modulation of the glycocalyx. Previous studies from the lab introduced synthesized heparan sulfate proteoglycans (HSPG) termed neo proteoglycans (NeoPGs) that mimic HS and have a high infinity for binding growth factors[18] (Figure 7). These neoPGs were used to promote the differentiation of embryonic stem cells (ESC) into neural precursor cells. A disaccharide library that mimics naturally occurring HS disaccharides was developed and utilized by Trieger et al. as the building blocks for the insertion of sulfated glycopolymer mimetics into the plasma membrane of preadipocytes via a fluorescently labeled lipid motif. HS-mimetics that are more negatively charged induce a stronger response when introduced to Ndst1$^{-/-}$ MEFs during the first three days of cellular differentiation. Heparin treated WT glucose uptake surpassed baseline levels

when stimulated with increasing concentrations of glycopolymer. The incorporation of the glycopolymers into Ndst1$^{-/-}$ cells completely restored glucose uptake capacity, surpassing that of WT cells (Figure 8B). The next step in the project is to selectively target preadipocytes by using an antibody mediated approach.

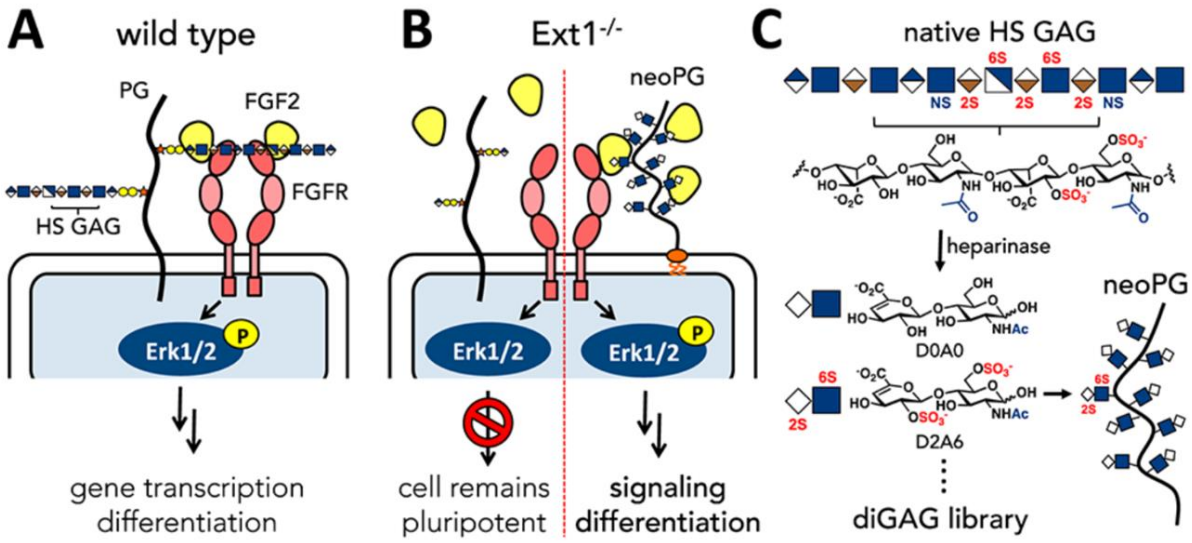

Figure 7: Glycocalyx Remodeling Strategy for Influencing Stem Cell Specification.
A. WT ESC: HSPGs are required for FGF signaling during development **B.** Synthetic neo-proteoglycans (neoPGs) attached to lipid anchors are introduced to surfaces of ESCs deficient in HS biosynthesis to rescue FGF signaling and enable differentiation. **C.** Glycan building blocks derived from native HS serve as growth factor recognition elements for neoPGs. 2-O sulfation is required for FGF2 binding and 6-O sulfation improves affinity for FGF2 binding. Sulfated neoPG D2A6 (disulfated) was able to restore FGF2 binding while non sulfated neoPG D0A0 did not show affinity for binding FGF2. Image from Huang, et al[18]

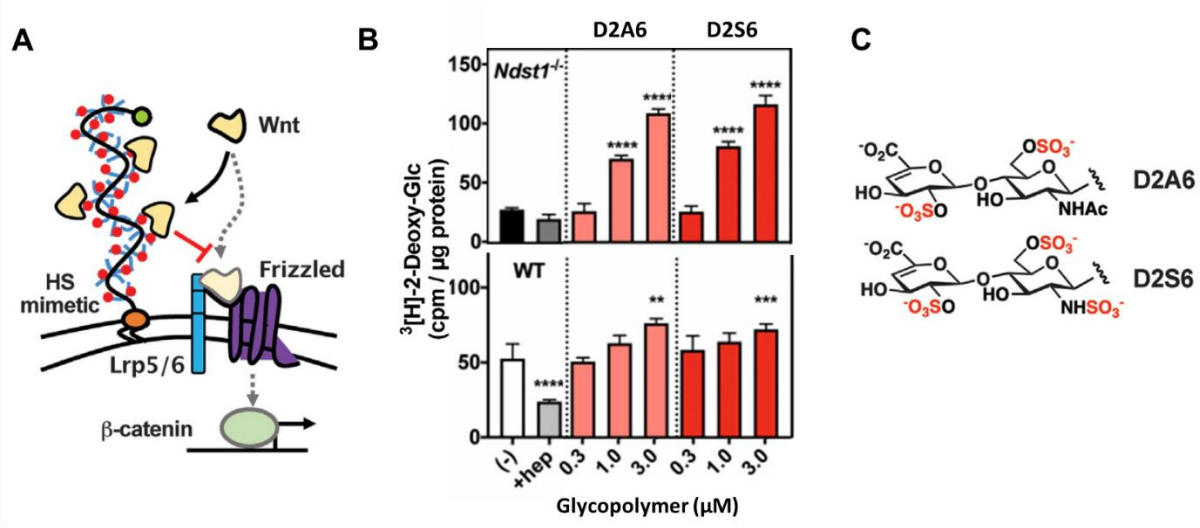

Figure 8: Differentiation with HS-Mimetics Increases Glucose Uptake of Mature Adipocytes
A. Synthetic glycopolymers bearing HS GAG disaccharide repeats were prepared and incorporated into the membranes of differentiating MEFs. Schematic of Wnt ligand sequestration by cell membrane anchored HS glycopolymers. **B.** Ndst1$^{-/-}$ and WT MEFs are treated with glycopolymer for 1 h at 37°C on day 0 to 3 of adipocyte differentiation. Sulfated glycopolymers D2A6 and D2S6 are able to dose-dependently enhance 3[H]-2deoxy-glucose uptake in differentiated adipocytes (day 6) (two-way ANOVA, n = 3). **C.** Selected HS GAG disaccharides D2A6 (disulfated), and D2S6 (trisulfated). Figure from Trieger et al[19].

Current HS-mimetics rely on lipid anchors for membrane insertion in tissue culture. This conjugation is nonspecific as lipid anchors can be found on the cell surface of many tissue types. The antibody handle addresses this limitation and has the potential to overcome specificity if this model were to move in vivo. Our lab used tetrameric streptavidin to conjugate heparin to biomolecules (unpublished). To evolve this technology, monomeric streptavidin (mSA) was isolated from E-coli and purified (unpublished). Using mSA prevents unwanted protein aggregation and allows for more precise analysis of cell surface interactions. Tyr-PEG$_4$-amine (S2) was coupled to heparin through reductive amination yielding a hep-tyr-PEG$_4$-amine complex termed Hep-Tyr, and subsequently added to mSA through tyrosinase mediated oxidation forming the mSA, heparin, tyr-PEG$_4$-amine glycoconjugate termed hep-mSA (unpublished). The biotin

binding site on the monomeric streptavidin is accessible and allows the attachment of biotinylated moieties, such as antibodies, fatty acids, and fluorescent probes.

Thesis Problem

This thesis aims to address the lack of specificity of the current glycocalyx engineering approach for producing adipocytes with enhanced glucose clearance capacity by establishing a novel class of HS-mimetics with the ability to specifically target preadipocytes in the initial stages of adipogenesis. Creating a targetable approach to regulate glucose uptake independently of insulin signaling could be a novel therapeutic treatment option for patients with T2D.

The focus of this thesis is to lay the foundation for such approach by addressing two specific challenges:

1) Identifying and validating a preadipocyte-specific cell-surface marker for targeted delivery of HS-mimetics during early stages of adipogenesis

and

2) Designing a HS-mimetic-antibody conjugate for preadipocyte targeting to regulate their differentiation toward adipocytes with enhanced glucose metabolism.

Together these findings will set the stage for future investigation of adipogenesis in vitro and eventually in animal models toward therapeutic development.

Materials and Methods

Cell Differentiation

WT and Ndst1$^{-/-}$ MEFs

Cells were differentiated to Days 0, 3, 6, and 8. Cells are seeded in culture plates at a density of 30k/cm^2 using Dulbecco's modified Eagle's medium (DMEM) supplemented with 10% fetal bovine serum (FBS) and 1% penicillin streptomycin (Standard DMEM). Throughout the differentiation, media is quenched every 48 hours. Cells are allowed to grow to confluency for 48-hrs (Day 0). On Day 0 cells are treated with differentiation media for 72-hours (Day 3). On day 3 and for the remaining duration of differentiation, cells are treated with insulin media.

Differentiation media consists of consists of Dexamethasone (0.1μM), 3-Isobutyl-1-methylaxanthine (IBMX, 450μM), Insulin (2μM), and Rosiglitazone (1μM) supplemented into standard DMEM. Insulin media consists of Insulin (2μM), and Rosiglitazone (1μM) supplemented into DMEM. Recipes are in Table 1.

NIH 3T3-L1 Fibroblasts

Cells were differentiated to Days 0, 2, 4, and 6. Cells are seeded in culture plates at a density of 60k/cm^2 using DMEM supplemented with 10% bovine calf serum (BCS) and 1% penicillin streptomycin. Throughout the differentiation, media is quenched every 48 hours. Cells are allowed to grow to confluency for 24 hours (Day -3), then allowed to arrest their growth for an additional 48 hours (Day 0). On day 0, cells are washed twice with DMEM supplemented with 10% FBS and treated with differentiation media for 48 hours (Day 2). On Day 2, cells are washed twice with DMEM supplemented with 10% FBS and treated with insulin media for 48 hours (Day 4). On Day 4 cells are washed twice

with DMEM supplemented with 10% FBS and are grown in maintenance media for the remaining duration of differentiation.

Differentiation Media consists of Dexamethasone (1μM), IBMX (0.5mM), Insulin (1μM), and Rosiglitazone (2μM) supplemented into standard DMEM. Insulin media consists of insulin (1μM) supplemented in standard DMEM. Maintenance media is Standard DMEM. Recipes are in Table 1.

Flow Cytometry

Cells were seeded in 6-well plates at a density of 30k/cm^2 (WT and Ndst1$^{-/-}$) or 60k/cm^2 (3T3-L1). After aspirating media from cells, they are lifted with 0.5mL of 10mM ETDA-DPBS solution for 10min at 37°C. Cells are washed once with 0.1% Bovine Serum Albumin BSA-DPBS wash buffer then counted using trypan blue and the countess cell counter. 100k cells for each condition/test are separated out and placed in an Eppendorf or designated well in a 96-well v-bottom plate. Cells are washed once and resuspended in 100μL of primary antibody, biotinylated anti CD140a (PDGFRα) for 1hr on a shaker (130rpm) at 4°C. Cells are centrifuged and washed twice, then incubated with Streptavidin-PE for 1hr at 4°C. Cells are centrifuged and washed twice before analyzing on BD FACS CANTO II. Data analysis was accomplished using FlowJo_v10.8.1 software. Statistical analysis was performed with GraphPad Prism 10 software.

Immunostaining

Cells were differentiated to Days 0, 3, 6, or 8 in a 24-well plate. After aspirating media from cells, they are fixed with 4% Paraformaldehyde (PFA) for 15 minutes. Cells are washed thrice with DPBS for 10 minutes, then incubated for 30 minutes with casein blocking buffer. Afterwards, cells are incubated with primary antibody, biotinylated anti-

PDGFRα overnight at 4°C. Following primary antibody incubation, cells are washed thrice with DPBS and subsequently incubated with streptavidin-PE for 1 hour at room temperature. Streptavidin is a protein that has a high infinity for biotin. Next, cells are washed once with DPBS and incubated with Hoechst nuclei stain for 10 minutes. After nuclei staining, cells are washed twice with DPBS if imaging on the same day and once with DPBS and fixed for a second time using 4% PFA for 10 minutes if imaging the next day. After fixation, cells are washed thrice with DPBS and imaged using the Keyence (BZ-X710) fluorescent microscope.

Cells were seeded on subsequent days to allow for same day analyses. When analyzing, at least three images from each well were taken.

HS-mimetic-antibody Conjugation

Chemoenzymatic synthesis of glycoconjugate starts with the reductive amination reaction of HS with sodium cyanoborohydride to covalently attach tyr-PEG_4-amine to HS. Hep-Tyr is then bound to the cysteine residue of mSA through an enzyme catalyzed reaction. This mSA-Hep conjugate is then incubated with biotinylated anti-PDGFRα overnight at 4°C to form the targeting HS-mimetic.

Western Blotting

Conjugates are loaded to Native Page Gel at constant concentrations. Tris Buffer (1%) is added to the holding cells. Gel is run at 200mV for 2hours. A power blotter is used to transfer the get to a polyvinylidene difluoride (PVDF) membrane. The membrane is blocked with blocking buffer for 1 hour at room temperature. Primary antibodies are incubated overnight at 4°C. The membrane is washed three times with DPBS supplemented with 0.1 % tween 20 and secondary antibodies are applied and incubated

for 1 hour at room temperature. The membrane is washed three times with DPBS before imaging.

Results

1) Identification and validation of a preadipocyte-specific cell-surface marker for targeted delivery of HS-mimetics during early stages of adipogenesis.

Heparan sulfate's ability to induce changes in metabolic activity is restricted to early differentiation; therefore, it is crucial to target a gene that is expressed during early adipogenesis and not expressed in mature adipocytes. For successful manipulation of the glycocalyx, the target must have a cell membrane bound localization for HS coupling ability. I began with literature reviews[31–33] and gathered a list of potential early adipogenic markers (Figure 3B). To further specify candidate targets, I utilized protein atlas (https://www.proteinatlas.org/) and eliminated transporters, secreted, and sole intracellular markers from the list. Consequently, I focused on PDGFRα and DLK1 (Pref-1) as potential candidates. To minimize off target effects in future in-vivo studies, tissue specificity was included in my search criteria. Searching for tissue specificity within the protein atlas interface, there was more data collected for PDGFRα than Pref1. Upon coming across an article inferring Pref-1 expression in the brain[34], I decided to start with PDGFRα as the cell surface marker.

Next, I validated the expression of PDGFRα in MEF preadipocyte progenitor cell lines (WT and Ndst1$^{-/-}$) during adipogenesis. This would give the baseline level of PDGFRα on the cells and confirm it fades as cells become mature adipocytes. The expression of PDGFRα was measured via flow cytometry (Figure 9A-B) and microscopy (Figure 10A-B). Initial flow cytometry results showed minimal PDGFRα expression on Day

0 of differentiation, which is incongruent with other findings[35]. I turned to Ndst1$^{-/-}$ cells for comparative analysis, and these cells gave a much more robust signal. Comparison of mRNA expression during adipogenesis revealed PDGFRα was much higher in Ndst1$^{-/-}$ MEFs than WT MEFs (Figure 9C). After optimizing the flow cytometry protocol, I performed time course analyses on both WT (Figure 9A) and Ndst1$^{-/-}$ (Figure 9B) MEFs. PDGFRα expression was assessed on Days 0, 3 and 6 of differentiation. In agreement with the mRNA analysis, PDGFRα expression on WT MEFs increased during the first 3 days of differentiation and declined as cells became mature adipocytes (Figure 9C). In contrast, the expression of PDGFRα by Ndst1$^{-/-}$ MEFs started high and decreased throughout differentiation. Fold change was measured by taking the geometric means and normalizing relative to background for mean fluorescence intensity (MFI) above background.

Figure 9. Evaluation of PDGFRα Expression During the Course of Adipogenesis
A. Histograms and bar graph representations of PDGFRα expression during adipogenesis in WT MEFs via flow cytometry. The expression is low on day 0, increases by day three and decreases by day 6. **B.** Histograms and bar graph representations of PDGFRα expression during adipogenesis in Ndst1$^{-/-}$ MEFs via flow cytometry **C.** PDGFRα mRNA of WT and Ndst1$^{-/-}$ MEFs. **D.** Histograms and bar graph representations of PDGFRα expression during adipogenesis in 3T3-L1 fibroblasts via flow cytometry.

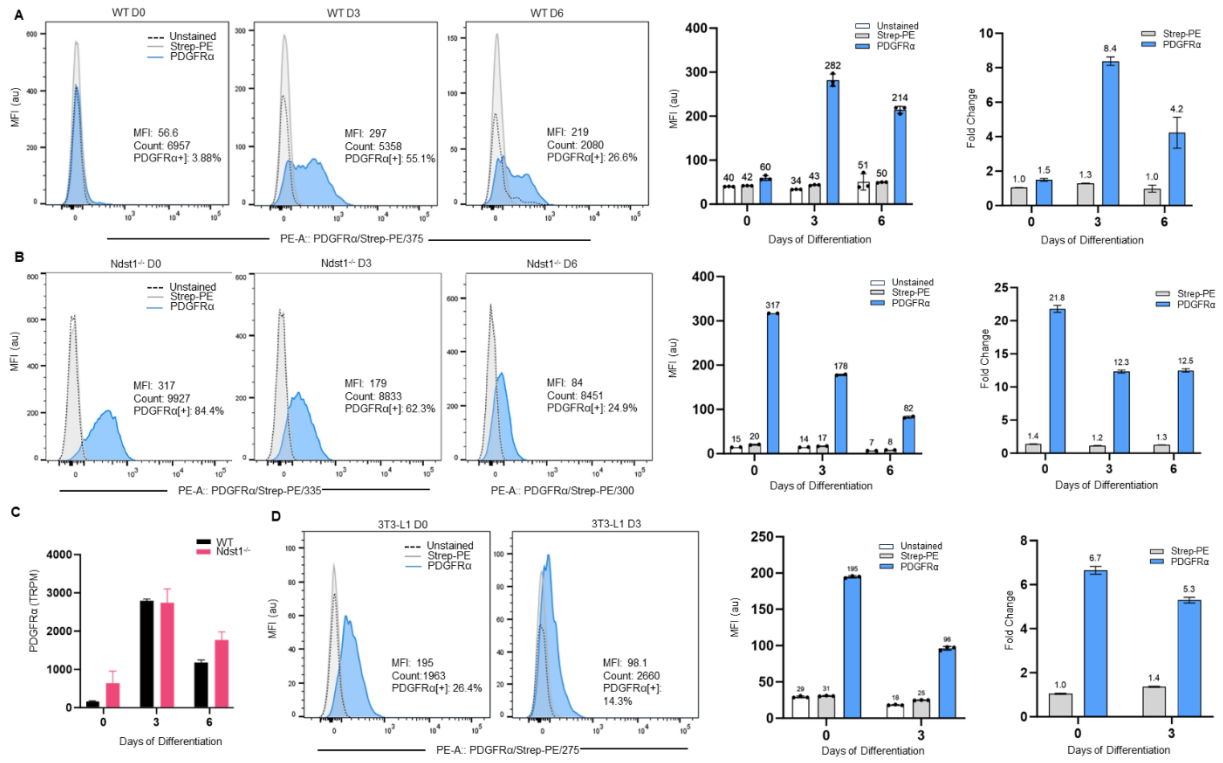

Immunocytochemical staining and fluorescence microscopy were performed to confirm trends of PDGFRα expression during differentiation in WT and Ndst1$^{-/-}$ MEFs (Figure 10A-B). It was also used to confirm initial flow cytometry results on WT MEFs, which suggested low PDGFRα expression during Day 0 of adipogenesis. Immunostaining and microscopy imaging were performed on Days 0 and 8 with or without membrane permeabilization (S1 Figure 1). Staining after membrane permeabilization was performed to assess total levels of PDGFRα expression, while non-permeabilizing conditions were used to detect only cell-surface localized receptors. To mirror flow cytometry time courses, immunocytochemistry was performed for Days 0, 3, and 6 of differentiation. Immunofluorescence (IF) was analyzed via ImageJ software by inverting images, adjusting the thresholds, and measuring the minimum, maximum, and mean gray values with the measuring tool within ImageJ interface. MFI and Standard Error of Mean (SEM)

were calculated by dividing positive mean for PDGFRα by positive mean for Hoechst (nuclei).

Visually, the expression of PDGFRα followed the trends seen in flow cytometry, however, the quantitative comparison of MFI values for both WT and Ndst1$^{-/-}$ MEFs throughout differentiation were not in line with flow cytometry results. WT MFIs ±SEM: 1.2 ±0.036, 1.063 ±0.034, and 1.139 ±0.032 on Days 0, 3, and 6 respectively. Ndst1$^{-/-}$ MFIs ±SEM: 1.062 ±0.034, 1.123 ±0.020, and 1.188 ±0.037 on days 0, 3, and 6 respectively. Together, the immunostaining results are inconclusive; however, the quantification method for this analysis is quite subjective and repeating the analysis using an alternative software may be worth exploring.

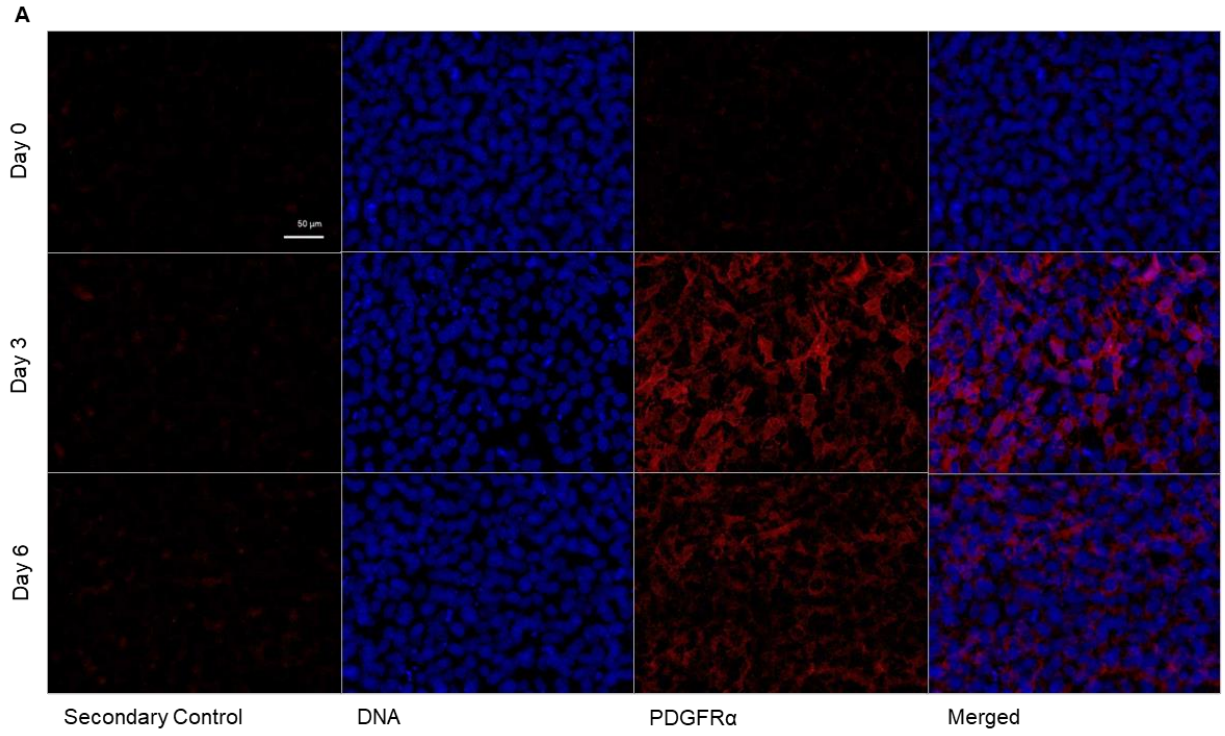

Figure 10: Immunostaining of PDGFRα Expression During the Course of Adipogenesis
A. Immunostaining for PDGFRα on WT MEFs on days 0, 3, and 6 of differentiation, MFIs are 1.2,1.063, and 1.139 respectively; the MFI values are not significant between the three stains. **B.** Immunostaining for PDGFRα expression on Ndst1-/- MEFs on days 0, 3, and 6 of differentiation. MFIs are 1.062,1.123, and 1.188 respectively; the MFI values are not significant between the three stains. **C.** Immunostaining of PDGFRα expression in 3T3-L1 fibroblasts on days 0, 3, and 6 of differentiation, MFIs are 1.030,1.052, and 1.053 respectively; the MFI values are not significant between the three stains. GraphPad Prism analysis: n=9 for all apart from $Ndst1^{-/-}$ day 6 where n=6.

Figure 10 Continued

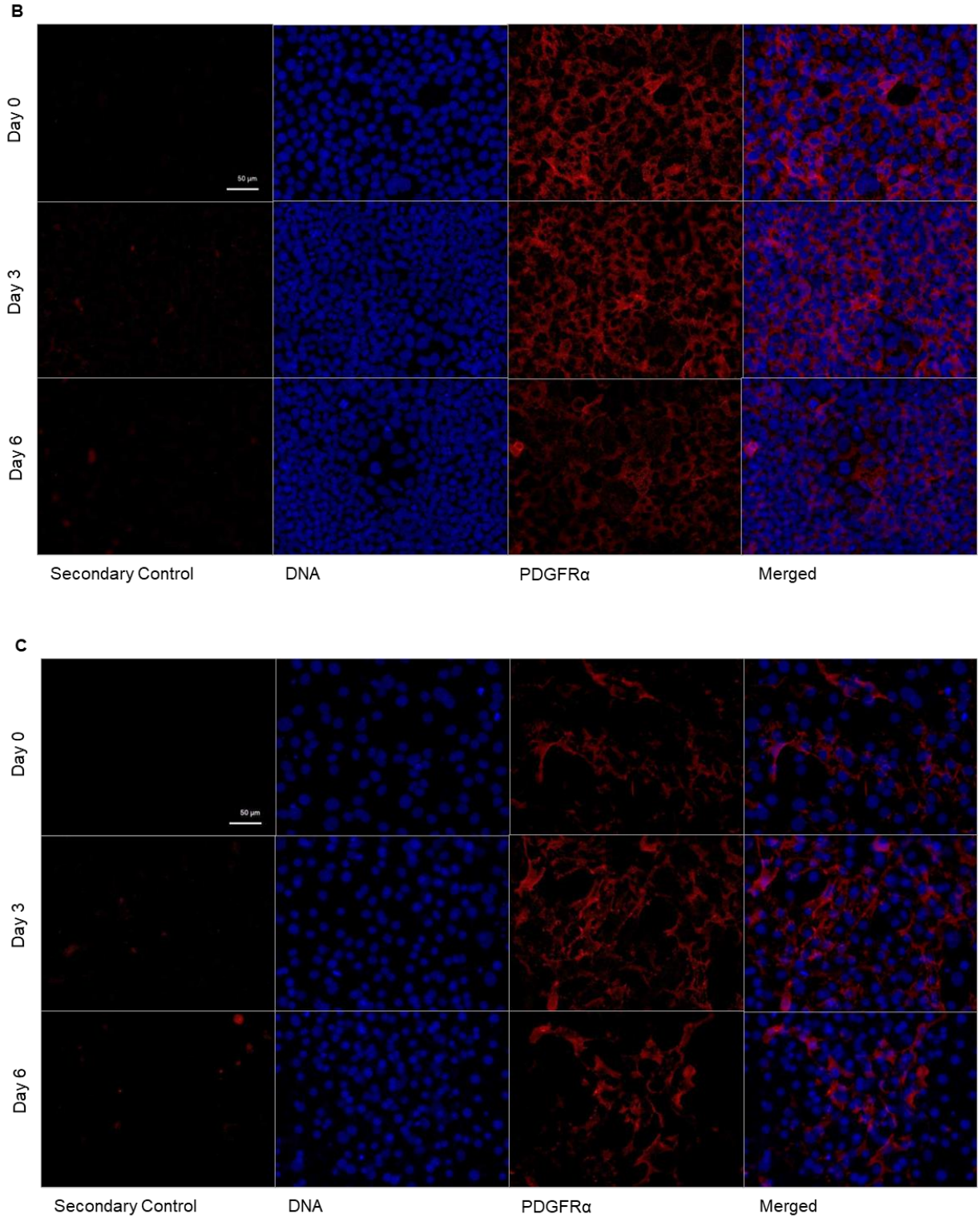

To explore if these results were reproducible in an established adipogenic cell model, I performed both flow cytometry and immunocytochemical staining on 3T3-L1 murine fibroblasts. The differentiation protocol is slightly different; but the flow cytometry results are comparable to Ndst1$^{-/-}$ MEFs (Figure 9C), with PDGFRα starting high at Day 0 and declining by Day 3. Cells could not be analyzed via flow cytometry beyond day 3 due to lipid droplet accumulation which caused the cells to float. Immunocytochemical staining (Figure 10C) showed an insignificant increase in the expression of PDGFRα over time, yielding normalized MFI ±SEM of 1.030 ±0.006, 1.053 ±0.005 and 1.052 ±0.005 on Days 0, 3, and 6 respectively.

In all previous experiments 1µL of biotinylated anti-PDGFRα antibody was diluted into 200µL of buffer. To produce a conjugate with that dilution factor would require an unreasonable amount of antibody. To overcome this, binding analysis was performed via flow cytometry. Serial dilutions (1:200, 1:500, 1:1000, 1:1500) of biotinylated anti-PDGFRα were incubated on cells for 1 hour at 4°C. Analysis of flow cytometry data resulted in a half maximal binding response (EC_{50}) value of 0.78nM (Figure 11). Dilutions correspond to the following concentrations 8.130, 3.120, 1.630, 1.080nM respectively. Cells stained with only Streptavidin-Phycoerythrin (Strep-PE) were used as the 0-concentration point.

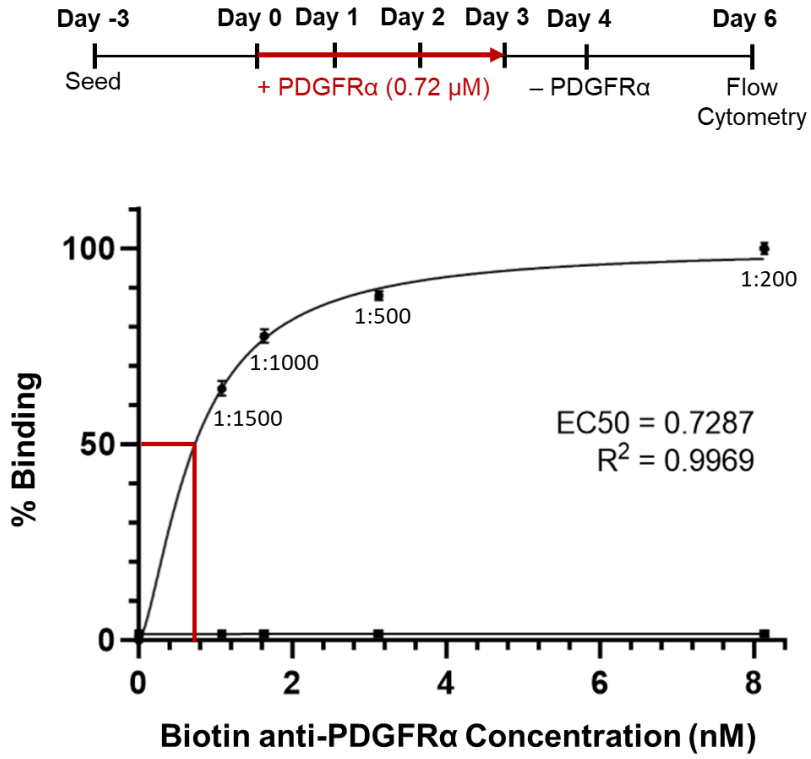

Figure 11: Binding Curve for Biotinylated anti-PDGFRα Antibody
Serial dilutions (1:200, 1:500. 1:1000, 1:1500) of biotinylated anti-PDGFRα were incubated for 1 hour at 4 °C and subsequently incubated with Strep-PE for 1 hour at 4°C. Flow cytometry data analyzes resulted in an EC_{50} of 0.78nM.

Before constructing the conjugate, 3T3-L1 cells were used to confirm that the biotinylated anti-PDGFRα antibody would not interfere with adipogenesis. Cells were seeded at 60k/cm^2 in a 24-well plate and cultured to Day 6 of differentiation. Biotinylated anti-PDGFRα antibody is introduced to the differentiation media on Days 0-3 at 0.78μM, the concentration of the antibody determined by titration as described above (Figure 11). During this 3-day period, the media is changed daily and reintroduced to biotinylated anti-PDGFRα. On day 2, cells are washed twice before adding insulin media containing the antibody. On day 4, cells were washed twice and kept in maintenance media for the remainder of the differentiation without the antibody. On day 6, cells are imaged for comparison. Visually, there were no apparent differences between cells with or without

the antibody and adipogenesis ensued (Figure 12). However, confirmation of adipogenic lineage formation via mRNA and histochemical analysis of adipogenic marker expression and glucose uptake should be completed to confirm the effects of the antibody are negligible. Finally, the full range of antibody concentrations will need to be assessed to confirm no deleterious effects on adipogenesis. Taken together, the data suggest that PDGFRα is a viable preadipocyte marker and biotinylated anti-PDGFRα antibody can be used as the affinity handle for HS-mimetics to engineer adipogenesis.

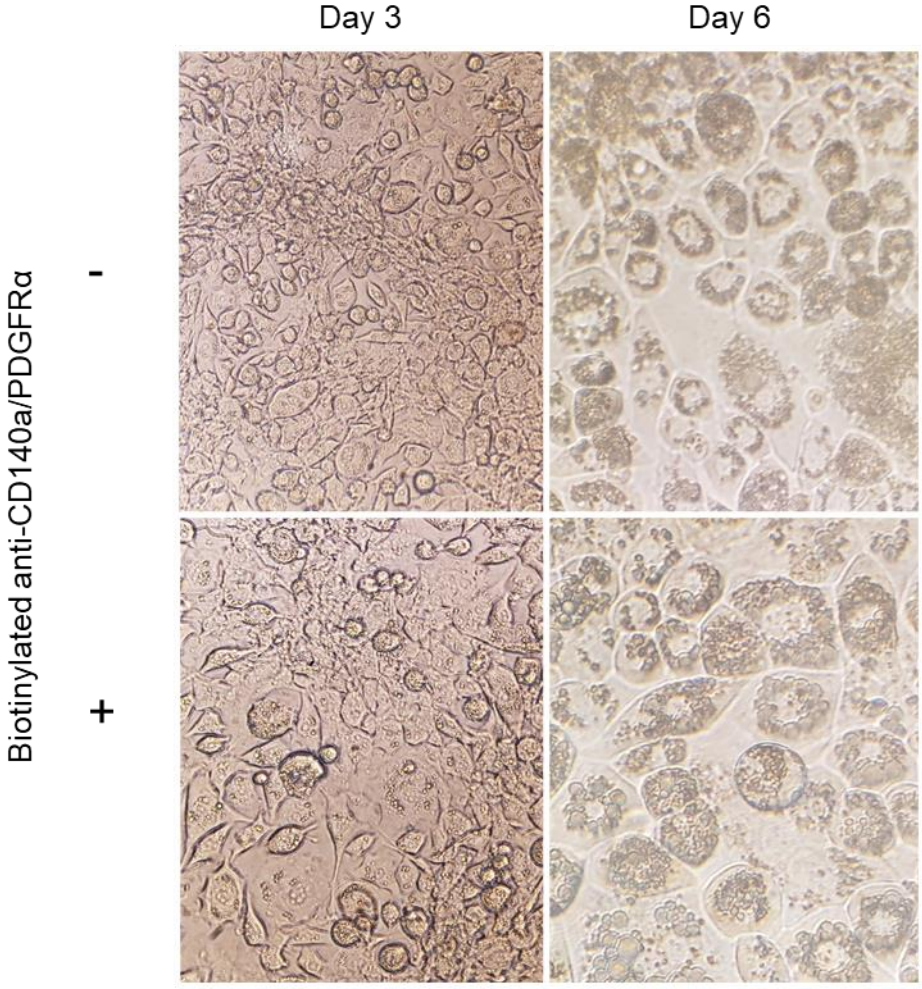

Figure 12: Differentiation with Biotinylated anti-PDGFRα Does Not Impair Lipid Accumulation
Images depict Day 3 and Day 6 of 3T3-L1 differentiation with and without biotinylated anti-PDGFRα. Day 3 images are magnified 20X and Day 6 images are magnified 40X. Images were taken by a phone camera.

2) Designing a HS-mimetic-antibody conjugate for preadipocytes targeting to regulate their differentiation toward adipocytes with enhanced glucose metabolism.

As mentioned previously, HS-mimetics produced by our lab utilize a lipid anchor to introduce conjugates into the membrane of cells. This new approach to creating HS-mimetics uses an antibody, which gives our mimetics a targeting capability. For the synthesis of the conjugates, heparin is used in place of HS as it is commercially available and has less variability than HS[28]. Also, instead of using tetrameric streptavidin, we use monomeric streptavidin (mSA). Tetrameric streptavidin (WT SA) is a protein that has a high infinity for biotin with four active biotin binding sites. WT SA has been used by our lab to conjugate heparin to other large biomolecules (unpublished). To enhance the quantification of hep-SA binding affinity, one active subunit of SA was isolated and purified from *E. coli* BL21(DE3)pLysS to generate mSA as seen in Supplementary File 3 (S3). This construct has only one active biotin binding site instead of the four that are present in WT SA and is used as the link between heparin and the targeting antibody.

Heparin was conjugated to mSA via a tyr-PEG_4-amine linker (Figure 13). Polyethylene glycol (PEG) is a poly ether that is used as a conjugation ligand for therapeutic delivery[36]. Our lab found that the addition of the PEG-4 linker to tyramine (Tyr-PEG_4-amine) is crucial for successful conjugation of biomolecules to heparin (unpublished). To conjugate heparin to mSA, first heparin is aminated at the reducing end's aldehyde via reductive amination, using sodium cyanoborohydride as the reducing agent. This reaction takes place overnight at 32°C and produces a conjugate between heparin and tyr-PEG_4-amine (Hep-Tyr). Next, Hep-Tyr is coupled to the cysteine residue

on mSA by Tyrosinase (abTYR) mediated oxidation. This reaction was developed recently and allows for quick, site specific conjugation of two biomolecules[37]. Prior to this advancement in protein-protein conjugation, proteins were coupled together using heterobifunctional crosslinking agents or biorthogonal click reactions[37]. This abTYR approach to coupling proteins is found to be more effective in our lab and therefore is used for our conjugation strategy. The mSA is added to a solution of Hep-TYR in phosphate buffer, abTYR is added to this solution and allowed to react for 2 hours at room temperature. This reaction produces the desired conjugated protein handle (hep-mSA) for our HS-mimetic.

To demonstrate the validity of hep-mSA, it was conjugated to a fluorescently labeled biotin molecule (Figure 14). From left to right, the first lane shows the conjugation of hep-mSA. The second lane demonstrates how Dithiothreitol (DTT) disrupts sulfate binding, thus no conjugate is formed. Lane three shows that without the tyrosinase activity the hep-mSA conjugate cannot form. And lane four shows that mSA binds biotin.

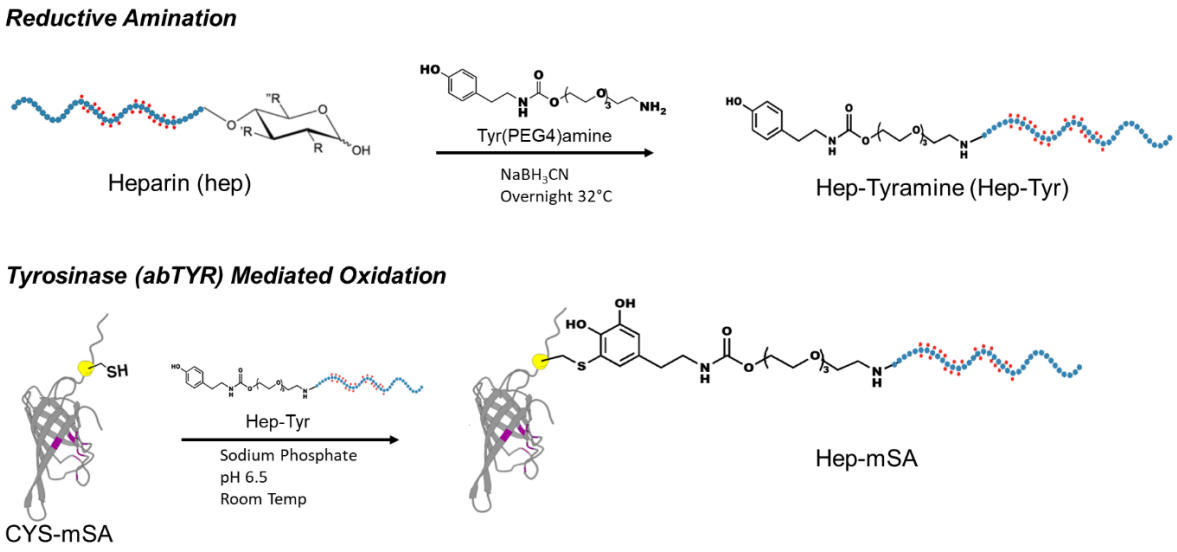

Figure 13: Chemoenzymatic Conjugation of Hep-mSA
Heparin is covalently linked to Tyr-PEG$_4$-amine through a reductive amination reaction yielding Hep-Tyr complex which is enzymatically coupled to mSA using tyrosinase to form Hep-mSA conjugate.

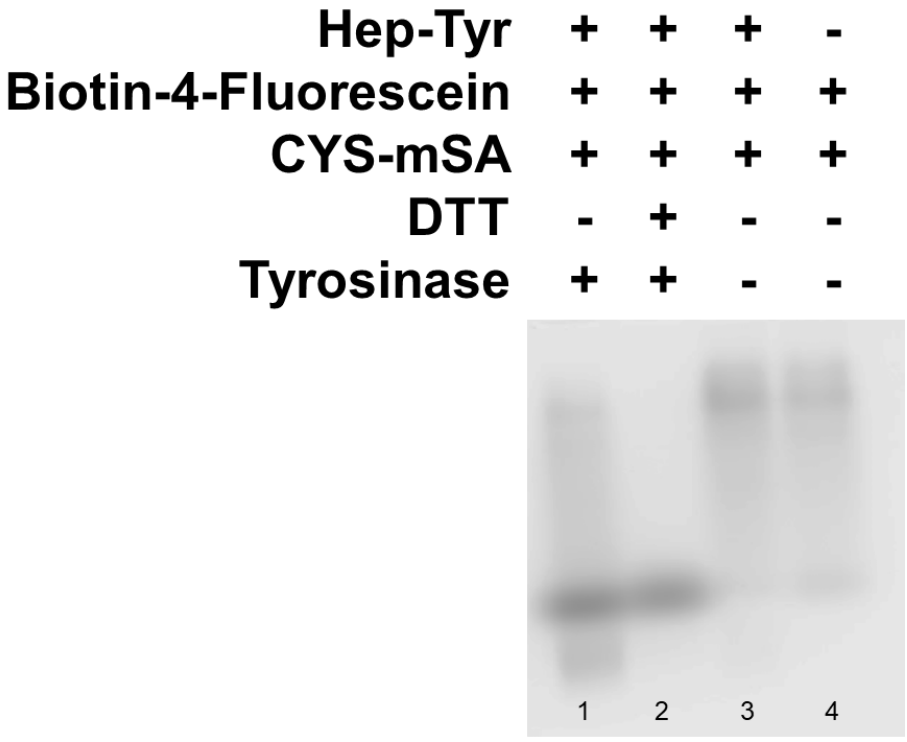

Figure 14: Validation of Hep-mSA conjugation with a Fluorescent Biotin Molecule
Hep-mSA was incubated with a fluorescently labeled biotin molecule. Without the tyrosinase enzyme (abTYR), the conjugate does not form. Adding DTT disrupts sulfate binding, and the conjugate is not formed.

Biotinylated anti-PDGFRα antibody was conjugated to hep-mSA by utilizing the SA affinity for biotin. Biotinylated anti-PDGFRα antibody was incubated with hep-mSA overnight at 4°C. To validate that the biotinylated anti-PDGFRα-hep-mSA HS-mimetic-antibody reaction occurred, two western-blotting strategies were used. The first approach analyzed the indirect formation of the conjugation between the hep-mSA and biotinylated anti-PDGFRα antibody by using a Native PAGE. After loading mSA and hep-mSA onto the gel and running it to completion, the gel is transferred to a membrane using a power blotter. After blocking, the membrane is incubated with biotinylated anti-PDGFRα antibody overnight at 4°C. After primary antibody incubation, the membrane is washed three times, and the fluorescently labeled secondary antibody (AF546) is added to the membrane for 1 hour at room temperature. This strategy resulted in an empty membrane, suggesting that the biotinylated anti-PDGFRα antibody did not react with mSA or hep-mSA. The second approach analyzed the direct conjugation of the ab-hep-mSA conjugate. Hep-mSA was separately incubated with primary (1°) biotinylated anti-PDGFRα and biotinylated anti-FGF2 (control) antibodies overnight at 4°C. After incubation, the protein was analyzed using a Native PAGE. Biotinylated anti-PDGFRα antibody, biotinylated anti-PDGFRα-hep-mSA, and biotinylated anti-PDGFRα-mSA (lanes 1-3 respectively), biotinylated anti-FGF2 antibody, biotinylated anti-FGF2-hep-mSA, and biotinylated anti-FGF2-mSA (lanes 4-6 respectively) are all ran through the gel. After completion of the run, the gel is transferred to a membrane and blocked for 1 hour at room temperature. The membrane is then incubated with secondary antibodies, AF546 for biotinylated anti-PDGFRα antibody and AF647 for biotinylated anti-FGF2 antibody. This resulted in an inconclusive result; for biotinylated anti-PDGFRα,

there is no apparent shift in lanes 1 and 2 but can arguably say there is a minute shift upward in lane 3 which would suggest that mSA only bound to the biotin on the primary antibody when it is unconjugated to heparin. Biotinylated anti-FGF2 has no shift in lanes 4 and 5 suggesting the biotinylated-anti-FGF2-hep-mSA conjugate did not form and has a higher molecular weight band in lane 6, suggesting the binding of biotinylated anti-FGF2 with mSA (Figure 14). This data suggests that neither antibody conjugated to hep-mSA, hence, there is an issue with the conjugation of hep-mSA to biotinylated antibodies. The antibody size, the accessibility of biotin on the antibody, or the net negative charge of heparin may be affecting the antibody-hep-mSA conjugation. This method needs to be optimized by assessing the potential causes of negative conjugation. Different methods of detection may also be employed to gain insight into how the complex is forming. For example, probing the blot for 10E4 – an antibody that recognizes HS – will show which samples have HS present.

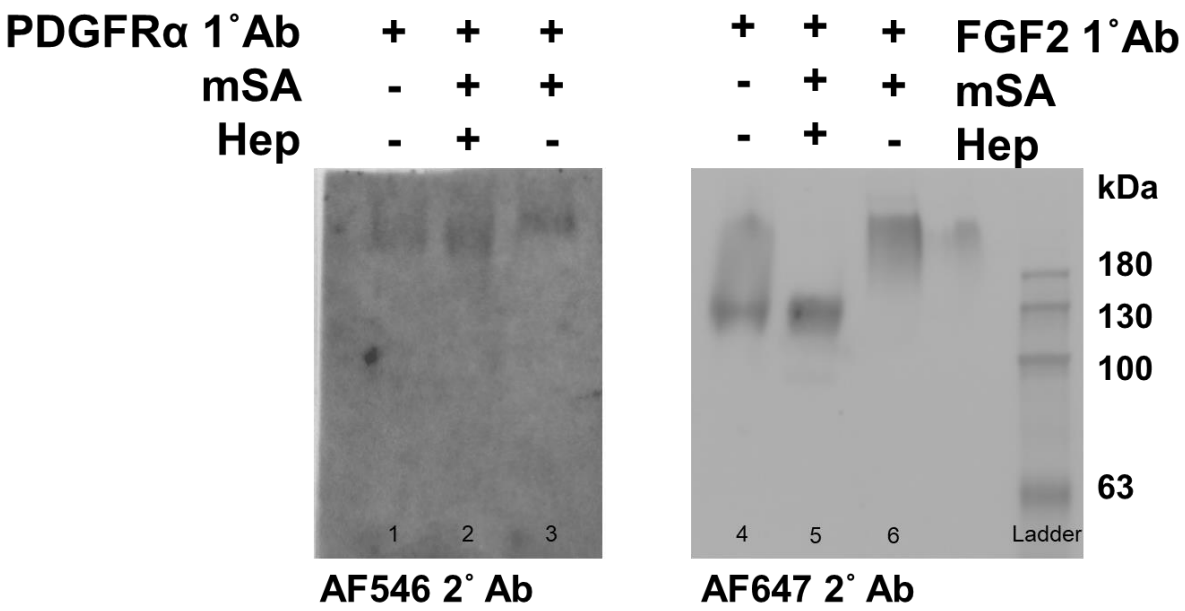

Figure 15: Western Blot of Antibody Mediated HS Conjugates
Western blot comparing biotinylated anti-PDGFRα-hep-mSA and biotinylated anti-FGF2-hep-mSA. PDGFRα was detected using 1:5000 AF546 secondary antibody (lanes 1-3) and FGF-2 was detected using 1:5000 AF647 secondary antibody (lanes 4-6).

Future Directions and Applications

Once biotinylated anti-PDGFRα antibody is effectively bound to hep-mSA, it can be used to target preadipocytes. Glucose uptake and lactate production studies can be done to confirm the Wnt sequestering functionality of HS. By adapting the hep-mSA-antibody conjugate, additional studies can be done to target mature adipocytes and explore how HS interacts with growth factors and affects downstream signaling pathways. As this antibody-mediated HS-mimetic becomes well established, studies can be done to analyze off targeting effects of this approach in live systems. The Hep-mSA conjugate has immense possibilities, as it can be adapted to many different biotinylated targets (antibodies, membrane proteins, lipids) which can be used to explore diverse cell types.

Conclusion

In this thesis, I have identified PDGFRα as a preadipocyte marker for potential conjugation to synthesized HS-mimetics, validated the expression level of PDGFRα in three cell models – WT MEFs, Ndst1$^{-/-}$ MEFs, and NIH 3T3-L1 preadipocyte murine cells, and began analyzing the effects of PDGFRα on adipogenesis. PDGFRα expression was measured and quantified via flow cytometry and immunocytochemical staining at various stages of differentiation. All three models show that biotinylated anti-PDGFRα is a viable antibody for targeting preadipocytes during early adipogenesis and although expression levels vary, PDGFRα trends in these models confirm that the window of opportunity to target preadipocytes for HS-mimetic incorporation is in the first 3 days of differentiation. Glycocalyx engineering is a promising therapeutic approach that is underdeveloped. More work is needed to complete this antibody mediated HS-mimetic for modulating glucose uptake in mature adipocytes; including the assessment of biotin accessibility on antibodies and completing mRNA analysis of adipogenic markers and glucose uptake assays after adipogenesis in the presence of biotinylated anti-PDGFRα antibody and the anti-PDGFRα-HS-mSA conjugate to confirm that incubation with each of these does not negatively interfere with adipogenesis.

Results section II is coauthored with Pravinkumar Choudhary, Julianna Follmar and Alexander Parmele. The thesis author was the primary author of this section.

Table 1: Differentiation Recipes for 10mL of DMEM supplemented with 10% FBS and 1% Penicillin streptomycin.

WT & Ndst1$^{-/-}$ Differentiation Media	**3T3-L1 Differentiation Media**
Dexamethasone(0.1μM): 25μL (40μM stock)	Dexamethasone(1μM): 10μL (1mM stock)
IBMX (450μM): 18μL (250mM stock)	IBMX (0.5mM): 20μL (250mM stock)
Insulin (2μM): 10μL (2mM stock)	Insulin (1μM): 5uL (2mM stock)
Rosiglitazone (1μM): 10μL (1mM stock)	Rosiglitazone (2μM): 20μL (1mM stock)
WT & Ndst1$^{-/-}$ Insulin Media	**3T3-L1 Insulin Media**
Insulin (2μM): 10μL (2mM stock)	Insulin (1μM): 5uL (2mM stock)
Rosiglitazone (2μM): 20μL (1mM stock	

Table 2: List of materials used for cell culture and experiments.

Materials	**Company**	**Item Number**
Biotin CD140a (PDGFRα)	R&D Systems	BAF1062
Bovine Serum Albumin Fraction V	Sigma Alderich	03117057001
Casein	Sigma Alderich	C3400
Cells: WT, Ndst1$^{-/-}$, 3T3-L1	Gifted by Gordts/Esko Lab	
Dexamethasone	Sigma Alderich	D4902
Dulbecco's Modified Eagle's Medium	Gibco	11965-092
Dulbecco's Phosphate Buffered Saline	Gibco	14190-144
Fetal Bovine Serum	Omega Scientific	FB-01
Hoechst 33342 Trihydrochloride	Invitrogen	H3570
IBMX	Sigma Alderich	I5879
Insulin Solution Human	Sigma Alderich	I9278
Paraformaldehyde (4%)	Thermo Fisher Scientific	J19943
Penicillin Streptomycin	Gibco	15140-122
Rosiglitazone	Cayman Chemical	71740
Streptavidin-PE	R&D Systems	F0040
Trypan Blue	Invitrogen	T10282
Ultrapure ETDA (0.5M)	Invitrogen	15575020

References

1. Harvey, I., Boudreau, A. & Stephens, J. M. Adipose tissue in health and disease. *Open Biol* **10,** 200291 (2020).

2. Sethi, J. K. & Vidal-Puig, A. J. Thematic review series: Adipocyte Biology. Adipose tissue function and plasticity orchestrate nutritional adaptation. *J Lipid Res* **48,** 1253–1262 (2007).

3. White, U. Adipose tissue expansion in obesity, health, and disease. *Front Cell Dev Biol* **11,** 1188844 (2023).

4. Congdon, P. & Amugsi, D. Editorial: The obesity epidemic: Causes, context, prevention. *Frontiers in Public Health* **10,** (2022).

5. Freeman, A. M., Acevedo, L. A. & Pennings, N. in *StatPearls* (StatPearls Publishing, 2024). at <http://www.ncbi.nlm.nih.gov/books/NBK507839/>

6. Lin, X., Xu, Y., Pan, X., Xu, J., Ding, Y., Sun, X., Song, X., Ren, Y. & Shan, P.-F. Global, regional, and national burden and trend of diabetes in 195 countries and territories: an analysis from 1990 to 2025. *Sci Rep* **10,** 14790 (2020).

7. Wagenknecht, L. E., Lawrence, J. M., Isom, S., Jensen, E. T., Dabelea, D., Liese, A. D., Dolan, L. M., Shah, A. S., Bellatorre, A., Sauder, K., Marcovina, S., Reynolds, K., Pihoker, C., Imperatore, G., Divers, J., & SEARCH for Diabetes in Youth study. Trends in incidence of youth-onset type 1 and type 2 diabetes in the USA, 2002-18: results from the population-based SEARCH for Diabetes in Youth study. *Lancet Diabetes Endocrinol* **11,** 242–250 (2023).

8. Shah, R. B., Patel, M., Maahs, D. M. & Shah, V. N. Insulin delivery methods: Past, present and future. *Int J Pharm Investig* **6,** 1–9 (2016).

9. Nasri, H. & Rafieian-Kopaei, M. Metformin: Current knowledge. *J Res Med Sci* **19,** 658–664 (2014).

10. Frías, J. P., Davies, M. J., Rosenstock, J., Pérez Manghi, F. C., Fernández Landó, L., Bergman, B. K., Liu, B., Cui, X., Brown, K., & SURPASS-2 Investigators. Tirzepatide versus Semaglutide Once Weekly in Patients with Type 2 Diabetes. *N Engl J Med* **385,** 503–515 (2021).

11. Pessentheiner, A. R., Ducasa, G. M. & Gordts, P. L. S. M. Proteoglycans in Obesity-Associated Metabolic Dysfunction and Meta-Inflammation. *Front Immunol* **11,** 769 (2020).

12. Haczeyni, F., Bell-Anderson, K. S. & Farrell, G. C. Causes and mechanisms of adipocyte enlargement and adipose expansion. *Obes Rev* **19,** 406–420 (2018).

13. Chen, Q., Zhang, Z., Luo, N. & Qi, Y. Elevated visceral adiposity index is associated with increased stroke prevalence and earlier age at first stroke onset: Based on a national cross-sectional study. *Front Endocrinol (Lausanne)* **13,** 1086936 (2023).

14. Sarjeant, K. & Stephens, J. M. Adipogenesis. *Cold Spring Harb Perspect Biol* **4,** a008417 (2012).

15. Richard, A. J., White, U., Elks, C. M. & Stephens, J. M. in *Endotext* (eds. Feingold, K. R., Anawalt, B., Blackman, M. R., Boyce, A., Chrousos, G., Corpas, E., de Herder, W. W., Dhatariya, K., Dungan, K., Hofland, J., Kalra, S., Kaltsas, G., Kapoor, N., Koch, C., Kopp, P., Korbonits, M., Kovacs, C. S., Kuohung, W., Laferrère, B., Levy, M., McGee, E. A., McLachlan, R., New, M., Purnell, J., Sahay, R., Shah, A. S., Singer, F., Sperling, M. A., Stratakis, C. A., Trence, D. L. & Wilson, D. P.) (MDText.com, Inc., 2000). at <http://www.ncbi.nlm.nih.gov/books/NBK555602/>

16. Morigny, P., Boucher, J., Arner, P. & Langin, D. Lipid and glucose metabolism in white adipocytes: pathways, dysfunction and therapeutics. *Nat Rev Endocrinol* **17,** 276–295 (2021).

17. Edwards, M. & Mohiuddin, S. S. in *StatPearls* (StatPearls Publishing, 2024). at <http://www.ncbi.nlm.nih.gov/books/NBK560564/>

18. Huang, M. L., Smith, R. A. A., Trieger, G. W. & Godula, K. Glycocalyx remodeling with proteoglycan mimetics promotes neural specification in embryonic stem cells. *J Am Chem Soc* **136,** 10565–10568 (2014).

19. Trieger, G. W., Pessentheiner, A. R., Purcell, S. C., Green, C. R., DeForest, N., Willert, K., Majithia, A. R., Metallo, C. M., Godula, K. & Gordts, P. L. S. M. Glycocalyx engineering with heparan sulfate mimetics attenuates Wnt activity during adipogenesis to promote glucose uptake and metabolism. *J Biol Chem* **299,** 104611 (2023).

20. Rizzatti, V., Boschi, F., Pedrotti, M., Zoico, E., Sbarbati, A. & Zamboni, M. Lipid Droplets Characterization in Adipocyte Differentiated 3T3-L1 Cells: Size and Optical Density Distribution. *Eur J Histochem* **57,** e24 (2013).

21. Zhao, X., Hu, H., Wang, C., Bai, L., Wang, Y., Wang, W. & Wang, J. A comparison of methods for effective differentiation of the frozen-thawed 3T3-L1 cells. *Analytical Biochemistry* **568,** 57–64 (2019).

22. Lindahl, U. & Kjellén, L. Pathophysiology of heparan sulphate: many diseases, few drugs. *Journal of Internal Medicine* **273,** 555–571 (2013).

23. Merry, C. L. R., Lindahl, U., Couchman, J. & Esko, J. D. in *Essentials of Glycobiology* (eds. Varki, A., Cummings, R. D., Esko, J. D., Stanley, P., Hart, G. W.,

Aebi, M., Mohnen, D., Kinoshita, T., Packer, N. H., Prestegard, J. H., Schnaar, R. L. & Seeberger, P. H.) (Cold Spring Harbor Laboratory Press, 2022). at <http://www.ncbi.nlm.nih.gov/books/NBK579925/>

24. Esko, J. D. & Selleck, S. B. Order out of chaos: assembly of ligand binding sites in heparan sulfate. *Annu Rev Biochem* **71,** 435–471 (2002).

25. Sarrazin, S., Lamanna, W. C. & Esko, J. D. Heparan Sulfate Proteoglycans. *Cold Spring Harbor Perspectives in Biology* **3,** a004952–a004952 (2011).

26. Mycroft-West, C. J., Abdelkarim, S., Duyvesteyn, H. M. E., Gandhi, N. S., Skidmore, M. A., Owens, R. J. & Wu, L. Structural and mechanistic characterization of bifunctional heparan sulfate N-deacetylase-N-sulfotransferase 1. *Nat Commun* **15,** 1326 (2024).

27. Gordts, P. L. S. M. & Esko, J. D. THE HEPARAN SULFATE PROTEOGLYCAN GRIP ON HYPERLIPIDEMIA AND ATHEROSCLEROSIS. *Matrix Biol* **71–72,** 262–282 (2018).

28. Shriver, Z., Capila, I., Venkataraman, G. & Sasisekharan, R. Heparin and Heparan Sulfate: Analyzing Structure and Microheterogeneity. *Handb Exp Pharmacol* 159–176 (2012). doi:10.1007/978-3-642-23056-1_8

29. Liu, J., Xiao, Q., Xiao, J., Niu, C., Li, Y., Zhang, X., Zhou, Z., Shu, G. & Yin, G. Wnt/β-catenin signalling: function, biological mechanisms, and therapeutic opportunities. *Sig Transduct Target Ther* **7,** 1–23 (2022).

30. de Winter, T. J. J. & Nusse, R. Running Against the Wnt: How Wnt/β-Catenin Suppresses Adipogenesis. *Front Cell Dev Biol* **9,** 627429 (2021).

31. Cawthorn, W. P., Scheller, E. L. & MacDougald, O. A. Adipose tissue stem cells meet preadipocyte commitment: going back to the future. *J Lipid Res* **53,** 227–246 (2012).

32. Hudak, C. S. & Sul, H. S. Pref-1, a Gatekeeper of Adipogenesis. *Front Endocrinol (Lausanne)* **4,** 79 (2013).

33. Ussar, S., Lee, K. Y., Dankel, S. N., Boucher, J., Haering, M.-F., Kleinridders, A., Thomou, T., Xue, R., Macotela, Y., Cypess, A. M., Tseng, Y.-H., Mellgren, G. & Kahn, C. R. Asc-1, PAT2 and P2RX5 are novel cell surface markers for white, beige and brown adipocytes. *Sci Transl Med* **6,** 247ra103 (2014).

34. Persson-Augner, D., Lee, Y.-W., Tovar, S., Dieguez, C. & Meister, B. Delta-Like 1 Homologue (DLK1) Protein in Neurons of the Arcuate Nucleus That Control Weight Homeostasis and Effect of Fasting on Hypothalamic DLK1 mRNA. *Neuroendocrinology* **100,** 209–220 (2014).

35. Vaziri, C. & Faller, D. V. Down-regulation of Platelet-derived Growth Factor Receptor Expression during Terminal Differentiation of 3T3-L1 Pre-adipocyte Fibroblasts*. *Journal of Biological Chemistry* **271,** 13642–13648 (1996).

36. Kolate, A., Baradia, D., Patil, S., Vhora, I., Kore, G. & Misra, A. PEG — A versatile conjugating ligand for drugs and drug delivery systems. *Journal of Controlled Release* **192,** 67–81 (2014).

37. Lobba, M. J., Fellmann, C., Marmelstein, A. M., Maza, J. C., Kissman, E. N., Robinson, S. A., Staahl, B. T., Urnes, C., Lew, R. J., Mogilevsky, C. S., Doudna, J. A. & Francis, M. B. Site-Specific Bioconjugation through Enzyme-Catalyzed Tyrosine–Cysteine Bond Formation. *ACS Cent. Sci.* **6,** 1564–1571 (2020).